Int. J. Heat Mass Transfer. Vol. 35, No. 5, pp. 1049–1058, 1992
Printed in Great Britain

0017–9310/92 $5.00 + 0.00
Pergamon Press Ltd

Rapid solidification following laser melting of pure metals—I. Study of flow field and role of convection

BISWAJIT BASU
Tata Research Development and Design Centre, 1, Mangaldas Road, Pune 411 001, India

and

A. W. DATE
Department of Mechanical Engineering, Indian Institute of Technology, Powai, Bombay 400 076, India

(*Received* 13 *June* 1990 *and in final form* 20 *May* 1991)

Abstract—This paper is concerned with the numerical predictions of characteristics of rapid solidification following laser melting. The numerical model is based on the enthalpy formulation to account for the latent heat release during solidification and the momentum equations are solved by the SIMPLE algorithm in the liquid domain only. With different laser powers (10^8 and 10^9 W m^{-2}) and interaction times, the flow field and the temperature distribution within the liquid pool during rapid solidification are studied for aluminium and steel. The flow field is observed to die out very soon after the laser beam is removed. At higher power, the liquid pool remains very deep in the case of aluminium for a relatively long time due to a large secondary vortex formed during melting. Although the shape of the interface is different, there is a marginal difference in the total solidification times with and without convection for both the metals.

1. INTRODUCTION

LASER surface melting allows selective heating and melting of the surface. This selective heating modifies the surface properties of the material due to rapid melting followed by rapid solidification. Due to intimate contact between the melt and the solid substrate, the rate of heat extraction during solidification is very fast, which results in very high cooling rates of the order of 10^5–10^8 K s^{-1} [1]. This leads to the fine microstructure and, in turn, to improved surface properties like better resistance to wear and corrosion [2].

It has been pointed out by various researchers [3–7] that fluid flow plays an important role during laser surface melting. Mehrabian *et al.* [3] first reported the importance of surface tension driven fluid flow when they observed the circular convection pattern in the microstructure of laser treated Al–4.5% Cu. Anthony and Cline [4] have shown the importance of surface tension driven fluid flow during laser melting through an analytical model in one dimension. Srinivasan and Basu [5] studied the same situation in a two-dimensional rectangular melt. They have shown that the fluid flow in a laser melted pool develops very fast and a moving laser melting problem can be analysed using a quasi-stationary approach.

Chan *et al.* [6–8], Kuo and Wang [9], Basu and Srinivasan [10] and Basu and Date [11, 12] reported numerical studies of the fluid flow during steady state and transient laser melting problems. Except for Kuo and Wang's [9] model, all the other studies were carried out in two dimensions. Kuo and Wang [9] studied the effect of a positive surface tension gradient which may occur due to impurities and observed a very deep melt pool. Basu and Srinivasan [10] and Basu and Date [11] have shown the two cell flow structures in the laser melted pool of steel and aluminium. Based on a parametric study of laser melting with varying power densities (10^8–10^9 W m^{-2}) and beam radii (0.5–2.0 mm), Basu and Date [12] identified critical values of the process parameters for aluminium and steel below which convection plays a negligible role.

Most of the rapid solidification studies after laser melting are based on the pure conduction model [13–16]. Hsu *et al.* [13, 14] and Kuo *et al.* [15] presented one-, two- and three-dimensional studies, respectively. Hsu *et al.* [13] found that the cooling rate was increased by two orders of magnitude when the absorbed power was increased by one order of magnitude. Sekhar *et al.* [16] studied laser melting and solidification of aluminium alloy and have shown that the average cooling rate at the top is higher than that at the bottom of the pool. Chan *et al.* [6] also reported a similar observation based on their cooling rate calculation at the end of melting. Ramarao and Sekhar [17] studied rapid solidification using a three-

NOMENCLATURE

B_f	boundary heating factor, qr_0C_p/k
Bi	Biot number, hr_0/k
C_p	specific heat [J kg^{-1} K^{-1}]
Gr	thermal Grashof number, $g\beta\Delta TL^3/\nu^2$
h	convective heat transfer coefficient [W m^{-2} K^{-1}]
H	enthalpy [J kg^{-1}]
H_{sat}	enthalpy of saturated solid [J kg^{-1}]
k	thermal conductivity [W m^{-1} K^{-1}]
Ma	Marangoni number, $U_R r_0/\alpha$
Nu	Nusselt number, hL/k_1
p	pressure [N m^{-2}]
Pr	Prandtl number, ν/α
q	laser heat flux [W m^{-2}]
r	space variable [m]
r_0	radius of the laser beam [m]
r_{max}	width of the laser melted pool
R_σ	surface tension Reynolds number, $U_R r_0/\nu$
R_r	radiation factor, $\sigma\varepsilon r_0(T_b^2+T_\infty^2)(T_b+T_\infty)/k$
Ste	Stefan number, $C_p(T_m-T_\infty)/\lambda$
t	time [s]
T	temperature [K]
U_R	characteristic velocity, $(d\sigma_s/dT)(\lambda/\mu C_p)$ [m s^{-1}]
V_r	radial velocity [m s^{-1}]
V_z	axial velocity [m s^{-1}]
z	space variable [m]
z_{max}	depth of the laser melted pool.

Greek symbols

α	thermal diffusivity [m^2 s^{-1}]
β	coefficient of volumetric expansion due to thermal gradient [K^{-1}]
ε	emissivity
θ	non-dimensional temperature
λ	latent heat of fusion [J kg^{-1}]
μ	dynamic viscosity [N m^{-2} s^{-1}]
ν	kinematic viscosity [m^2 s^{-1}]
ρ	density [kg m^{-3}]
σ	Stefan–Boltzmann constant, 5.6697×10^{-8} W m^{-2} K^{-4}
σ_s	surface tension [N m^{-1}]
τ	non-dimensional time
τ_{melt}	non-dimensional interaction time
ϕ	non-dimensional enthalpy.

Subscripts

I	interface
l	liquid
m	melting point
s	solid
sat	saturated
∞	surrounding.

Superscript

*	dimensional value.

dimensional conduction model and observed that the solid/liquid temperature gradient falls from a very high value in the initial period of the transient to a low steady value. They compared the predicted cooling rates with the measured ones and found the agreement to be within 10%. Paul and Debroy [18] reported the first comprehensive study of solidification following laser melting with convection for welding application. They studied melting of pure iron with 0.127 mm beam radius (i.e. a focused beam) and high power densities (5.0×10^8–10^{10} W m^{-2}), which are typical in laser welding applications. The predicted cooling rates matched very well with the experimental observations. They also studied the free surface deformation during melting and solidification in the presence of convection.

A detailed study of rapid solidification after laser melting in the presence of fluid flow has not yet been reported. Paul and Debroy's [18] analysis is directed to laser welding. In this paper, the role of fluid flow during rapid solidification is presented for laser surface melting under various beam powers, melting times and materials. The flow field is studied using streamlines to highlight the changing nature of the flow structure with beam parameters, materials and time. The movement of the solid/liquid interface is predicted both with and without convection.

2. THE NUMERICAL MODEL

The present model is developed for a cross-section perpendicular to the laser scanning direction, as shown in Fig. 1. The numerical model is described in detail by the present authors elsewhere [11] and, hence, a brief description of the model will be presented.

The model is based on the following assumptions (discussed in detail by Basu and Date [11]):

(i) the heat transfer and the fluid flow are primarily in the r and z directions;

(ii) all properties except the surface tension are independent of temperature;

(iii) the free surface of the melt is flat;

(iv) the laser beam is stationary;

(v) the flow in the melt is laminar;

(vi) the buoyancy force is of negligible order of magnitude;

(vii) the heat flux at the boundary represents the

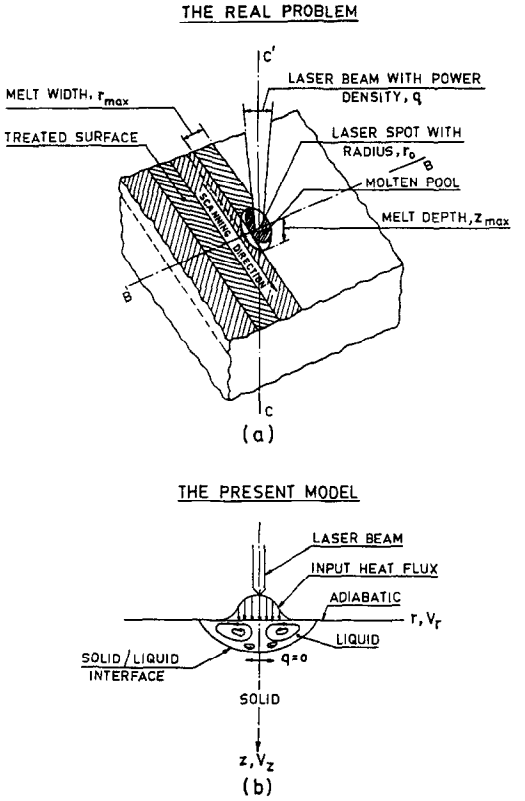

FIG. 1. Schematic representation of the laser surface melting along with the process parameters. (a) The real problem. (b) The model along the BB'CC' plane.

net heat input to the material after allowing for the surface reflectivity.

Using the following dimensionless variables

$$r = r^*/r_0; \quad z = z^*/r_0; \quad p = p^*/\rho U_R^2;$$
$$\phi = (H - H_{sat})/\lambda; \quad \theta = C_p(T - T_m)/\lambda;$$
$$V_r = V_r^*/U_R; \quad V_z = V_z^*/U_R; \quad \tau = t\alpha/r_0^2;$$
$$Ma = U_R r_0/\alpha; \quad R_a = U_R r_0/\nu;$$
$$Ste = C_P(T_m - T_\infty)/\lambda; \quad B_f = q r_0 C_p/k\lambda$$

the governing equations take the following form:

Energy equation

$$\frac{\partial \phi}{\partial \tau} + Ma\left[\frac{1}{r}\frac{\partial}{\partial r}(rV_r\phi) + \frac{\partial}{\partial z}(V_z\phi)\right] = \frac{1}{r}\frac{\partial}{\partial r}\left(kr\frac{\partial \theta}{\partial r}\right) + \left(\frac{\partial}{\partial z}\left(k\frac{\partial \theta}{\partial z}\right)\right) \quad (1)$$

r-Momentum equation

$$\frac{1}{Ma}\frac{\partial V_r}{\partial \tau} + \frac{1}{r}\frac{\partial}{\partial r}(rV_r^2) + \frac{\partial}{\partial z}(V_rV_z) = -\frac{\partial p}{\partial r} + \frac{1}{R_a}\left[\frac{\partial}{\partial r}\left\{\frac{1}{r}\frac{\partial}{\partial r}(rV_r)\right\} + \left(\frac{\partial}{\partial z}\frac{\partial V_r}{\partial z}\right)\right] \quad (2)$$

z-Momentum equation

$$\frac{1}{Ma}\frac{\partial V_z}{\partial \tau} + \frac{1}{r}\frac{\partial}{\partial r}(rV_rV_z) + \frac{\partial}{\partial z}(V_z^2) = -\frac{\partial p}{\partial r} + \frac{1}{R_a}\left[\frac{1}{r}\frac{\partial}{\partial r}\left(r\frac{\partial V_z}{\partial r}\right) + \left(\frac{\partial}{\partial z}\frac{\partial V_z}{\partial z}\right)\right] \quad (3)$$

Continuity equation

$$\frac{1}{r}\frac{\partial}{\partial r}(rV_r) + \frac{\partial V_z}{\partial z} = 0. \quad (4)$$

The corresponding boundary conditions are as follows:

$$\text{at } r = 0, \frac{\partial \theta}{\partial r} = \frac{\partial V_z}{\partial r} = V_r = 0; \quad 0 < z < \infty \quad (5)$$

$$\text{at } r = \infty, \theta = -Ste; \quad 0 < z < \infty \quad (6)$$

$$\left.\begin{aligned} &\text{at } z = 0, -k\frac{\partial \theta}{\partial z} = B_f \exp(-2r^2); \quad 0 < r < 1 \\ &\qquad = 0; \qquad\qquad 1 < r < \infty \\ &k\frac{\partial \theta}{\partial z} = (Bi + R_F)(Ste + \theta); \quad 0 < r < \infty \\ &\qquad \text{(for details see Appendix)} \\ &\frac{-\partial V_r}{\partial z} = \frac{\partial \theta}{\partial r}, V_z = 0; \quad 0 < r < r_{max} \end{aligned}\right\} \quad (7)$$

$$\text{at } z = \infty, \theta = -Ste; \quad 0 < r < \infty. \quad (8)$$

The initial conditions for melting are as follows:

$$\theta = -Ste; \quad V_r = V_z = 0; \quad \tau = 0, \quad 0 < r < \infty, \quad 0 < z < \infty. \quad (9)$$

The solidification calculations are initiated from different values of the interaction time, τ_{melt}.

Equations (1)–(4), along with the generalized enthalpy–temperature relationship introduced by Basu and Date [11], boundary and initial conditions, thus represent the laser melting and the solidification problem under transient conditions.

The governing equations are solved by a control volume-based finite difference method [19]. The algebraic equations resulting from the finite difference formulations are solved by a point by point (Gauss–Seidel type) iterative method satisfying the enthalpy–temperature relationship depending on the state of the control volume [11]. The enthalpy, velocities, pressure and pressure correction are underrelaxed by a relaxation factor of 0.8. The convergence at each time-level is checked using the fractional change and the residual error criterion [11]. All the numerical computations are carried out with 38×38 non-uniform grids with very fine grids below the beam and coarse ones away from the beam. A dimensionless time-step of 0.005 is found to be necessary to obtain stable solutions. The numerical model thus developed is validated by simu-

lating an electron beam experiment with aluminium alloy [11].

3. THE PARAMETERS STUDIED

The process parameters for the solidification study are as follows [11]:

q = beam power = 4×10^8 and 7.5×10^8 W m^{-2}
r_0 = beam radius = 2.0 mm
material = steel and aluminium
and τ_{melt} = melting time.

Since the results of the different radii, keeping beam power density constant, are similar [12], solidification studies are carried out with a single beam radius. The melting solution is fed as the initial condition for the solidification study. For each set of process parameters (i.e. beam specifications and material), a different melting time (τ_{melt}) is selected. For a moving beam, the interaction time is defined as the time during which the laser beam moves a distance of one diameter. The non-dimensional process parameters corresponding to the chosen beam characteristics and material properties are shown in Table 1.

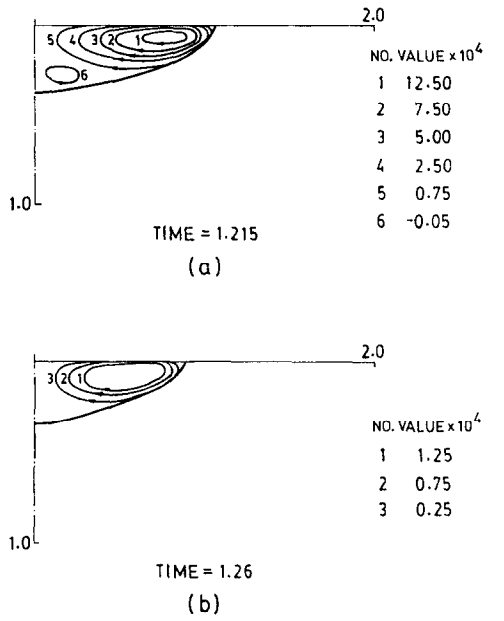

FIG. 2. Transient streamline and pool shapes for steel with a laser of 4.0×10^8 W m^{-2} power density and 2 mm radius for $\tau_{melt} = 1.215$.

4. RESULTS AND DISCUSSION

4.1. *Transient flow pattern and interface shape*

4.1.1. *Steel.* Figures 2 and 3 show the transient streamline for a beam of 2 mm radius and 4×10^8 W m^{-2} at two interaction times, $\tau_{melt} = 1.215$ and 1.985, respectively. At the time of initiation of solidification, the flow pattern shows the existence of two contra-rotating cells (Figs. 2(a) and 3(a)). Within a very short time span, it can be seen that the streamline values fall sharply (Figs. 2(b) and 3(b)) and the secondary cell disappears. This suggests that in the absence of the input heat flux, the fluid flow near the free surface neutralizes the surface temperature gradient. The convective flow due to high free surface velocity enhances the energy transfer at the free surface, i.e. from the centre of the pool (high temperature zone) towards the surface (low temperature zone), and, as a result, the temperature gradient at the free surface reduces. Since the surface temperature gradient is the driving force for the convection, the fluid flow generated during melting thus rapidly decays during solidification.

Figures 4–6 show the transient streamlines for a higher beam power of 7.5×10^8 W m^{-2} with different melting times: 1.365, 1.835 and 5.235, respectively. The beam radius is again 2.0 mm. The trend of the results is similar to the low power case except that the time span for the secondary cell to die out is more than that of the low power case. Due to the higher power of the beam, the superheat level attained is

Table 1.

		Aluminium	Steel
(i)	R_a	701 000.0	23 040.0
(ii)	Ma	6912.0	1806.0
(iii)	Pr	0.01	0.078
(iv)	Ste	1.6732	3.2516
(v)	B_i	20.0, 37.47	28.94, 54.27

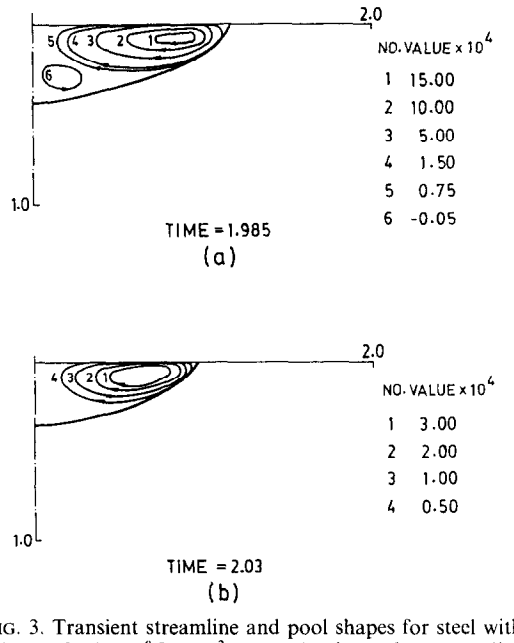

FIG. 3. Transient streamline and pool shapes for steel with a laser of 4.0×10^8 W m^{-2} power density and 2 mm radius for $\tau_{melt} = 1.985$.

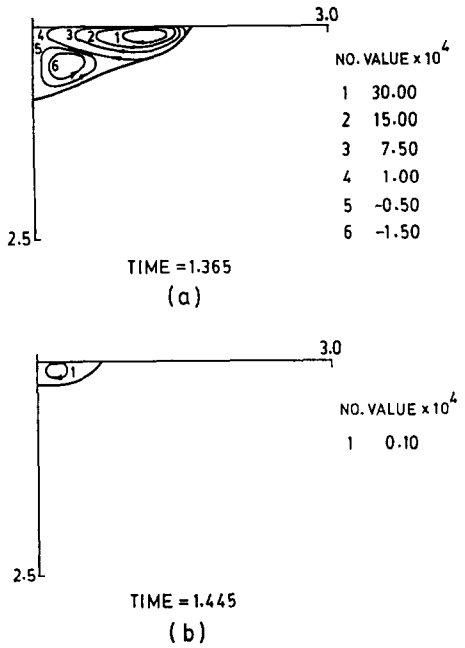

FIG. 4. Transient streamline and pool shapes for steel with a laser of 7.5×10^8 W m^{-2} power density and 2 mm radius for $\tau_{melt} = 1.365$.

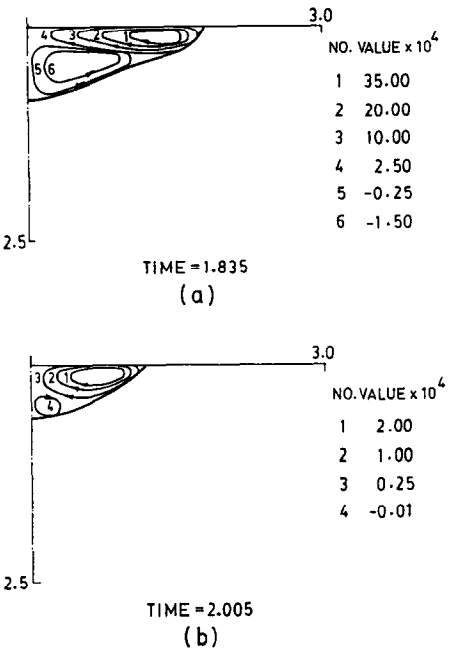

FIG. 5. Transient streamline and pool shapes for steel with a laser of 7.5×10^8 W m^{-2} power density and 2 mm radius for $\tau_{melt} = 1.835$.

higher, which results in a relative delay in the initiation of solidification.

4.1.2. *Aluminium.* Figures 7 and 8 show the streamlines for a beam of 2.0 mm radius and 4.0×10^8 W m^{-2} power density with different melting times: 1.715 and 1.875, respectively. Compared with the results for steel of the same power, the flow pattern shows the existence of a relatively stronger secondary cell at similar differential time, i.e. $\Delta\tau = \tau - \tau_{melt}$. Because of the lower *Pr* for aluminium, the rate of neutralization of the surface temperature gradient is slower for aluminium than for steel and as a result the rate of decrease of the flow field is smaller. Also, the Stefan number of aluminium (= 1.6732) is lower than that of steel (= 3.2516). This results in a slower rate of movement of the interface than that for steel and, thus, the pool shape remains deep while solidifying, resulting in the existence of the secondary cells. The two-cell flow pattern thus has more effect on aluminium than on steel. Figure 8 shows the change in the flow pattern for a higher melting time ($\tau_{melt} = 1.875$). The solidifying flow patterns are similar in nature (see Figs. 7(b) and 8(b)), except that a stronger cell is present in the case of $\tau_{melt} = 1.875$ after a time span of $\Delta\tau = 0.162$ than that of the lower τ_{melt} (=1.715) at the end of a similar time span ($\Delta\tau = 0.165$). This is due to the stronger flow and deeper pool for the case of higher τ_{melt}. Figure 7(c) shows that the secondary cell vanishes with a very weak flow when $\tau = 1.975$ for $\tau_{melt} = 1.715$, i.e. within a time span of 0.26 the flow dies out.

The streamlines with $\tau_{melt} = 2.895$ and 7.595 are shown in Figs. 9 and 10, respectively, for a beam of 2.0 mm radius and 7.5×10^8 W m^{-2} power density. During the onset of solidification, the flow pattern consists of large secondary cells in a deep pool. It can be seen from Fig. 9(b) that the shape of the molten

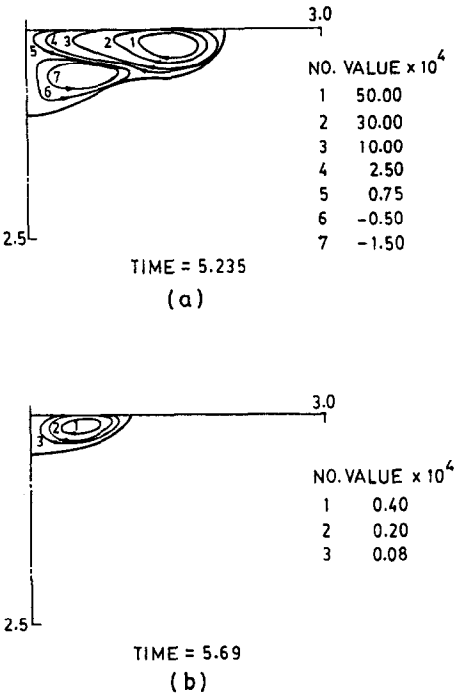

FIG. 6. Transient streamline and pool shape for steel with a laser of 7.5×10^8 W m^{-2} power density and 2 mm radius for $\tau_{melt} = 5.235$.

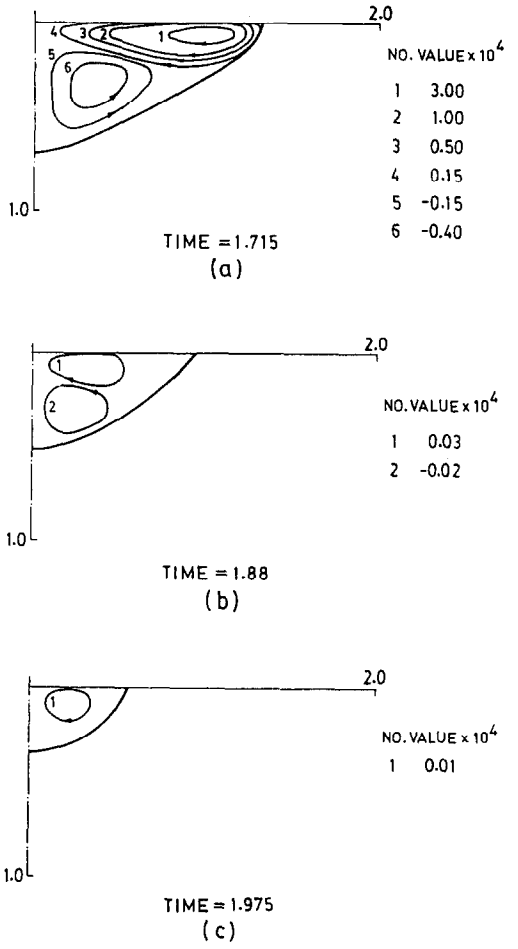

FIG. 7. Transient streamline and pool shapes for aluminium with a laser of 4.0×10^8 W m^{-2} power density and 2 mm radius for $\tau_{melt} = 1.715$.

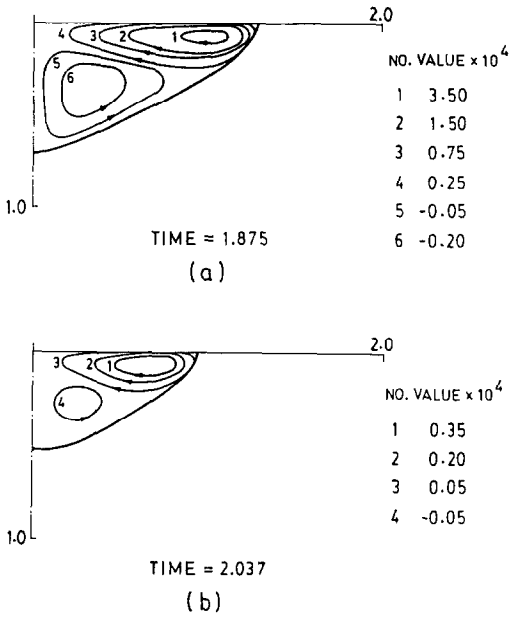

FIG. 8. Transient streamline and pool shapes for aluminium with a laser of 4.0×10^8 W m^{-2} power density and 2 mm radius for $\tau_{melt} = 1.875$.

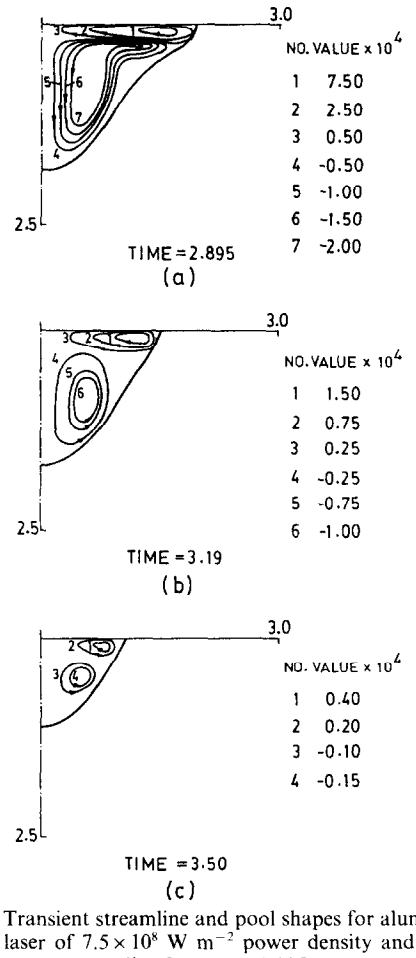

FIG. 9. Transient streamline and pool shapes for aluminium with a laser of 7.5×10^8 W m^{-2} power density and 2 mm radius for $\tau_{melt} = 2.895$.

pool changes dramatically at $\tau = 3.19$ when $\tau_{melt} = 2.895$. The interesting point to note is that the interface moves faster along the radial direction than along the vertical direction during this time span. This results in a deep pool, unlike all the other cases, and the secondary flow pattern is found to be different. The secondary flow brings the superheat from the top of the pool to the interfacial region. The primary cell does the same, i.e. superheat rejection, near the top surface. Because of the presence of the large secondary cells, the interface movement along the line of symmetry is slower in the present case. At $\tau = 3.5$, also, the pool shape is deep and shows the existence of a large but weak secondary cell. The trend of the results is similar for the higher melting time case, as can be seen in Fig. 10.

The secondary cells thus significantly affect the interface movement for aluminium with higher power. In the absence of secondary cells or the presence of weak secondary cells, the nature of interface movement is similar, i.e. aluminium with lower power and steel.

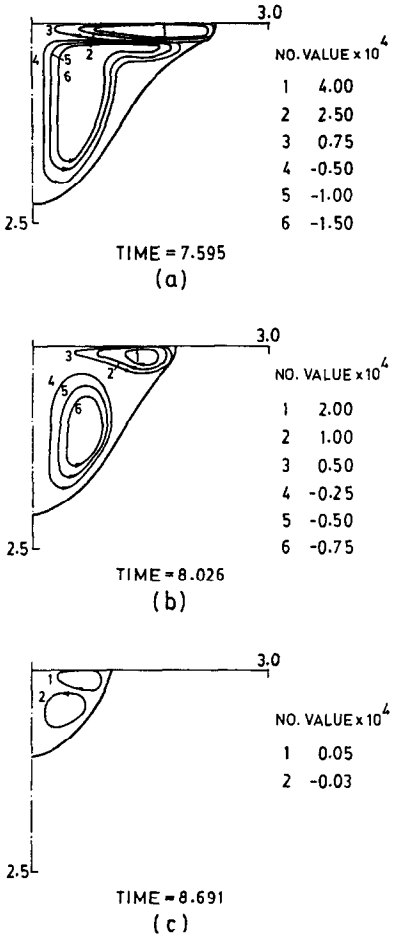

FIG. 10. Transient streamline and pool shapes for aluminium with a laser of 7.5×10^8 W m^{-2} power density and 2 mm radius for $\tau_{melt} = 7.595$.

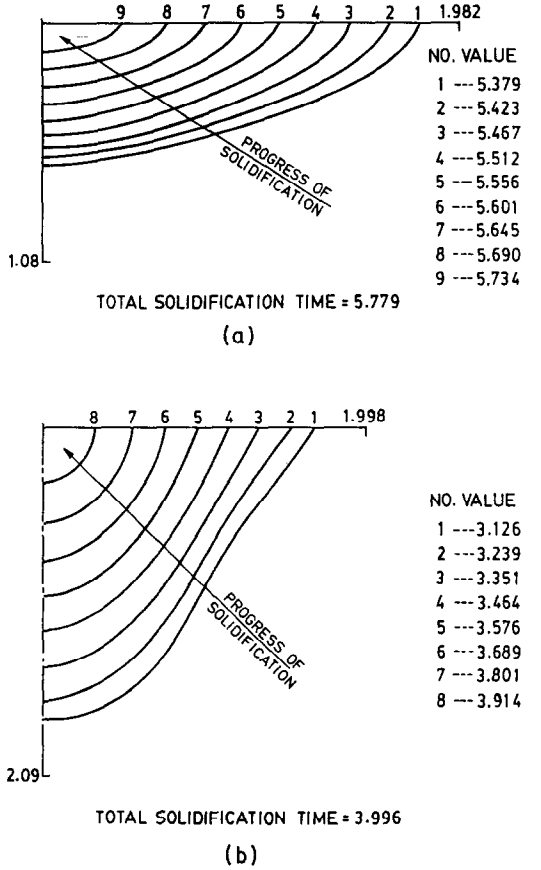

FIG. 11. Transient interface positions with convection till total solidification with a laser of 7.5×10^8 W m^{-2} power density and 2 mm radius. (a) Steel with $\tau_{melt} = 5.235$. (b) Aluminium with $\tau_{melt} = 2.895$.

4.2. *Transient interface position with and without convection*

4.2.1. *With convection.* Figure 11(a) shows the transient interface positions for steel with a beam of 7.5×10^8 W m^{-2} power density and 2.0 mm radius with convection. For $\tau_{melt} = 5.235$, the interface locations are plotted with equal time intervals ($= 0.044$). During the initial stage (i.e. $\tau = 5.379$, 5.423 and 5.467), it can be seen that the interface movement is slower. The speed of the interface gradually increases with time and the melt collapses suddenly at the end of solidification. This can be seen from the pool shape at $\tau = 5.734$ while the total solidification is at $\tau = 5.779$, i.e. within a time span of 0.045. From the point of view of the solidified microstructure, the microstructure will be relatively coarser at the bottom of the pool (i.e. the region of slow interface movement) with increasing fineness towards the top of the pool when the interface speed increases.

The transient interface positions for aluminium with the same beam specifications are shown in Fig. 11(b). Similar results are obtained for aluminium except for the slower movement of the interface (the time interval of the plot is 0.1125). This is due to the smaller *Ste* (1.6732) of aluminium than that of steel (3.2516).

4.2.2. *Comparison between conduction and convection solutions.* Figures 12(a) and (b) show the transient interface locations with and without convection for a beam of 2.0 mm radius and 4.0×10^8 and 7.5×10^8 W m^{-2} power densities, respectively. Near the line of symmetry, the conduction interface always lags behind the convection interface. On the other hand, near the free surface the conduction interface is ahead of the convection interface during the initial period of solidification, but the trend reverses with time. With the same initial temperature gradient across the solid/liquid interface, the initial interface movement will be faster in the pure conduction case because of the absence of convection, which would otherwise increase the temperature near the interface region. With the increase in time, the convection interface moves faster because of the faster rate of superheat removal which takes place during the initial period. This effect is not seen near the line of symmetry where a relatively weak flow exists. As a result of this efficient

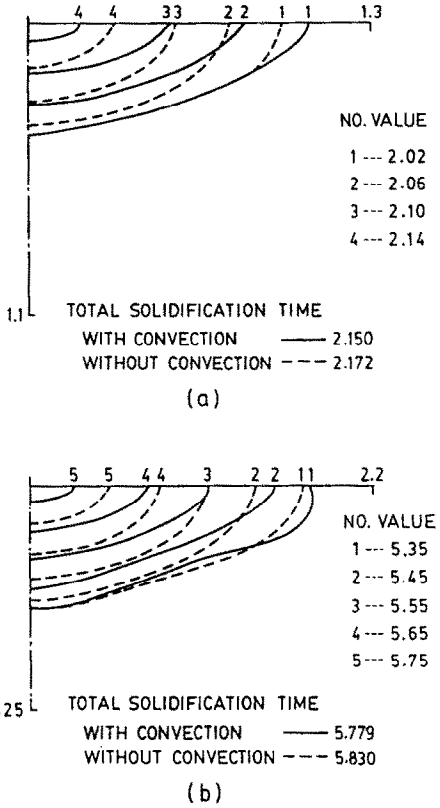

FIG. 12. Transient interface position with and without convection till total solidification for steel with a laser of 2 mm radius. (a) 4.0×10^8 W m^{-2} power density and $\tau_{melt} = 1.985$. (b) 7.5×10^8 W m^{-2} power density and $\tau_{melt} = 5.235$.

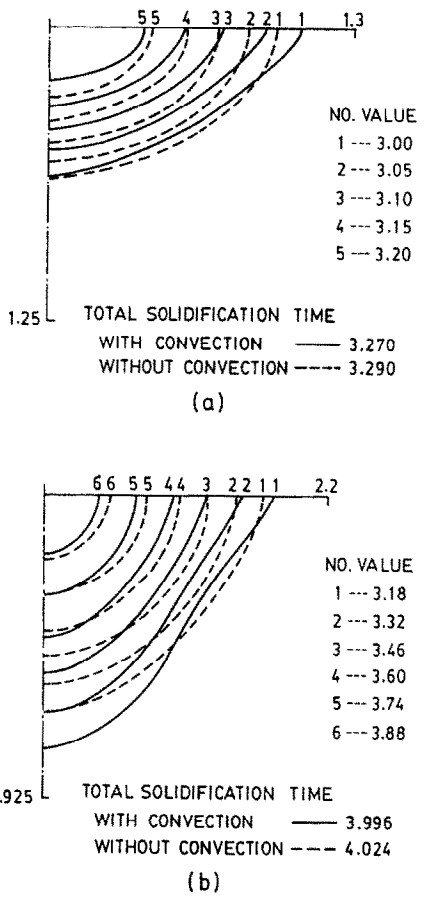

FIG. 13. Transient interface position with and without convection till total solidification for aluminium with a laser of 2 mm radius. (a) 4.0×10^8 W m^{-2} power density and $\tau_{melt} = 2.9$. (b) 7.5×10^8 W m^{-2} power density and $\tau_{melt} = 2.895$.

superheat removal, the total solidification time is always lower with convection than with conduction.

The transient interface positions with and without convection for aluminium with a 2.00 mm radius beam are shown in Figs. 13(a) and (b) for power densities of 4×10^8 and 7.5×10^8 W m^{-2}, respectively. Unlike steel, the difference between conduction and convection interface locations is less in the case of aluminium. This is because of the lower Pr (0.01) of aluminium which means a smaller effect of convection in superheat removal. From Fig. 13(a), it can be seen that the interface positions near the line of symmetry with and without convection also show the same trend as that along the top surface. Because of the stronger secondary cells, the effect of convection is therefore dominant along the line of symmetry.

Except during the initial stage of solidification, the shape of the interface with and without convection is similar. Due to the presence of strong convection, the interface shapes with convection are distorted from that with pure conduction during the initial stage of solidification. At higher times when the flow dies out, the shape of the interface with and without convection becomes similar (see Figs. 12(b) and 13(b)). The difference in the movement of the interface with and without convection is essentially due to the faster removal of superheat with convection. The difference in the total solidification time with and without convection is negligible for aluminium and marginally greater for steel than for aluminium.

5. CONCLUSIONS

The conclusions of this work can be summarized as follows.

(i) In the absence of input heat flux, the flow neutralized the top surface temperature gradient which is the driving force of the flow. As a result, the fluid flow dies out very quickly during solidification.

(ii) For steel, the flow pattern shows that the secondary cell disappears, resulting in a pool of primary cells only and the pool becomes shallower with time. The flow field and pool shape are similar for aluminium in the lower power case (i.e. 4×10^8 W m^{-2}). In the case of aluminium at higher power (7.5×10^8 W m^{-2}), the pool remains deep due to a very large secondary cell.

(iii) The solid/liquid interface movement is slow during the initial transient and very fast during the final stage when the pool collapses suddenly. The resulting microstructure will be fine at the top and coarse at the bottom.

(iv) From the comparison of the total solidification times with and without convection, the effect of flow during solidification is found to be negligible for aluminium and marginal for steel. Except during the initial stage of solidification, the interface shapes with and without convection are nearly identical.

Acknowledgements—The authors thank Prof. E. C. Subbarao, Director, Tata Research Development and Design Centre, for his encouragement. This work was supported by a project from the Defence Research and Development Organization, New Delhi.

REFERENCES

1. M. Allemen, *Laser Beam Interaction With Materials*. Springer, New York (1987).
2. S. T. Picraux and L. E. Pope, Tailored surface modification by ion implantation and laser treatments, *Science* **226**, 615–622 (1984).
3. R. Mehrabian, S. Kou, S. C. Hsu and A. Munitz, Laser surface melting and solidification. In *Laser–Solid Interaction and Laser Processing* (Edited by S. D. Ferris, H. J. Leamy and J. M. Pat). Materials Research Society, Boston (1979).
4. T. R. Anthony and H. E. Cline, Surface rippling induced by surface tension gradients during laser surface melting and alloying, *J. Appl. Phys.* **48**, 3888–3894 (1977).
5. J. Srinivasan and B. Basu, A numerical study of thermocapillary flow in a rectangular cavity during laser melting, *Int. J. Heat Mass Transfer* **29**, 563–572 (1986).
6. C. Chan, J. Mazumder and M. M. Chen, A two dimensional transient model for convection in laser melted pool, *Metall. Trans.* **15A**, 2175–2184 (1984).
7. C. Chan, J. Muzumder and M. M. Chen, A model for surface tension driven fluid flow in laser surface alloying. In *Lasers in Materials Processing* (Edited by E. A. Metzbower), pp. 150–157. American Society of Metals, Ohio (1983).
8. C. Chan, J. Mazumder and M. M. Chen, Three dimensional model for convection in laser melted pool. Presented at the 5th Int. Congress on the Lasers and Electro-optics, San Francisco, California (1985).
9. S. Kuo and Y. H. Wang, Three dimensional convection in laser melted pool, *Metall. Trans.* **17A**, 2265–2270 (1986).
10. B. Basu and J. Srinivasan, A numerical study of steady state laser melting problem, *Int. J. Heat Mass Transfer* **31**, 2331–2337 (1988).
11. B. Basu and A. W. Date, Numerical study of steady state and transient laser melting problem—I. Characteristics of flow field and heat transfer, *Int. J. Heat Mass Transfer* **33**, 1149–1163 (1990).
12. B. Basu and A. W. Date, Numerical study of steady state and transient laser melting problem—II. Effect of process parameters, *Int. J. Heat Mass Transfer* **33**, 1165–1175 (1990).
13. S. C. Hsu, S. Chakraborty and R. Mehrabian, Rapid melting and solidification of a surface layer, *Metall. Trans.* **9B**, 221–229 (1978).
14. S. C. Hsu, S. Kuo and R. Mehrabian, Rapid melting and solidification due to a stationary heat flux, *Metall. Trans.* **11B**, 24–28 (1980).
15. S. Kuo, S. C. Hsu and R. Mehrabian, Rapid melting and solidification due to a moving heat flux, *Metall. Trans.* **12B**, 33–45 (1981).
16. J. A. Sekhar, S. Kuo and R. Mehrabian, Heat flow model for surface melting and solidification of an alloy, *Metall. Trans.* **14A**, 1169–1177 (1984).
17. K. V. Ramarao and J. A. Sekhar, Unsteady rapid solidification with a moving heat source, *Acta Metall.* **35**, 81–87 (1986).
18. A. Paul and T. Debroy, Free surface flow and heat transfer in conduction mode laser welding, *Metall. Trans.* **19B**, 851–858 (1988).
19. S. V. Patankar, *Numerical Heat Transfer and Fluid Flow*. Hemisphere, New York (1980).
20. W. M. Kays and M. Crawford, *Convective Heat Mass Transfer*. Tata McGraw-Hill, New Delhi (1983).
21. E. R. Eckert and M. D. Drake, *Analysis of Heat and Mass Transfer*. Hemisphere, Tokyo (1972).

APPENDIX

Surface loss condition during the solidification after laser melting

The heat loss from the surface is by both convection and radiation. The total loss is therefore given by

$$q_1 = q_{\text{conv}} + q_{\text{rad}}. \tag{A1}$$

The normalized form of the total loss condition is as follows:

$$k\frac{\partial\theta}{\partial z} = (Bi + R_F)(Ste + \theta|_{z=0}). \tag{A2}$$

Calculation of the Biot number (Bi)

The convective heat loss is due to free convection from the top surface. A standard correlation is used to determine the convective heat transfer coefficient. For a horizontal surface, the heat transfer coefficient due to the free convection is as follows [20]:

$$Nu_L = 0.54(Gr \cdot Pr)^{1/4}$$
$$2.2 \times 10^4 < Gr \cdot Pr < 8.0 \times 10^6. \tag{A3}$$

For the present problem

L = reference length = $6.5r_0$ = 13.0 mm
β = volumetric coefficient of thermal expansion = $1.0/T$

(since air is an ideal gas and T is in K)

ΔT = reference temperature difference
= 1600 K for steel
= 700 K for aluminium

ν = kinematic viscosity of air
= 3.08×10^{-4} m^2 s^{-1} at 1800 K for steel
= 9.93×10^{-5} m^2 s^{-1} at 900 K for aluminium

(source: Eckert and Drake [21]).

Hence

Gr = 1220.0 for the case of steel
= 5134.0 for the case of aluminium.

Prandtl number

$$Pr \text{ at } 1800\text{ K} = 0.704$$
$$Pr \text{ at } 700\text{ K} = 0.684.$$

So

$Gr \cdot Pr$ = 860.0 for the case of steel.
= 3512.0 for the case of aluminium.

Although $(Gr \cdot Pr)$ is below the limit as specified in equation (A3), we still use this equation as the effect of this heat loss is very small, as can be seen from the Biot numbers below. Using equation (A3)

h = 32.53 W m^{-2} K^{-1} for the case of steel
= 24.53 W m^{-2} K^{-1} for the case of aluminium.

The corresponding Biot numbers are as follows:

$Bi = 0.001$ for the case of steel
$= 0.0004$ for the case of aluminium.

Calculation of R_F

The emissivity values of polished steel and aluminium are 0.35 and 0.26, respectively [21]. Hence

$R_F = 0.0046$ for the case of steel when the surface temperature is 1800 K.
$= 0.0003$ for the case of aluminium when the surface temperature is 900 K.

SOLIDIFICATION RAPIDE APRES FUSION LASER DE METAUX PURS—I. ETUDE DU CHAMP D'ECOULEMENT ET ROLE DE LA CONVECTION

Résumé—On prédit numériquement les caractéristiques d'une solidification rapide qui suit une fusion LASER. Le modèle numérique est basé sur la formulation enthalpique pour tenir compte de la chaleur latente lâchée pendant la solidification et les équations de quantité de mouvement sont résolues par l'algorithme SIMPLE dans le domaine liquide seul. On étudie pour l'aluminium et l'acier, avec différentes puissances laser (10^8 et 10^9 W m^{-2}) et des temps d'interaction, le champ d'écoulement et la distribution de température dans le bain liquide pendant la solidification rapide. Le champ d'écoulement s'éteint peu après que le faisceau laser est ôté. A forte puissance, le bain liquide reste profond dans le cas de l'aluminium, pour un temps relativement long à cause d'un grand vortex secondaire formé pendant la fusion. Bien que la forme de l'interface soit différente, il n'y a qu'une différence marginale dans les temps de solidification totale avec et sans convection pour les deux métaux.

SCHNELLE VERFESTIGUNG NACH DEM AUFSCHMELZEN REINER METALLE MITTELS LASER—I. UNTERSUCHUNG DES STRÖMUNGSFELDES UND DIE ROLLE DER KONVEKTION

Zusammenfassung—Die vorliegende Arbeit befaßt sich mit der numerischen Berechnung der schnellen Erstarrung nach einem Aufschmelzvorgang mittels Laser. Das numerische Modell berücksichtigt die mit der Erstarrung verbundenen Wärmequellen mit Hilfe einer Enthalpie Formulierung. Die Impulsgleichungen werden mit Hilfe des SIMPLE-Algorithmus nur im Flüssigkeitsgebiet gelöst. Das Strömungsfeld und die Temperaturverteilung in der Flüssigkeit wird für die schnelle Erstarrung von Aluminium und Stahl bei unterschiedlicher Laserleistung (10^8 und 10^9 W m^{-2}) und Einwirkungszeit untersucht. Es zeigt sich, daß das Strömungsfeld sehr schnell nach Abschalten des Laserstrahls zur Ruhe kommt. Bei größeren Leistungen bleibt die Flüssigkeit im Fall von Aluminium für eine relativ lange Zeit sehr tief. Dies wird auf einen großen Sekundärwirbel zurückgeführt, der während des Schmelzens entsteht. Obwohl die Form der Grenzfläche unterschiedlich ist, gibt es bei beiden Metallen nur einen verschwindend kleinen Unterschied zwischen den Verfestigungszeiten mit und ohne Konvektion.

БЫСТРОЕ ЗАТВЕРДЕВАНИЕ ЧИСТЫХ МЕТАЛЛОВ ПОСЛЕ ЛАЗЕРНОЙ ПЛАВКИ—I. ИССЛЕДОВАНИЕ ПОЛЯ ТЕЧЕНИЯ И РОЛИ КОНВЕКЦИИ

Аннотация—Численно определяются характеристики быстрого затвердевания после лазерной ния сохранения испульса решаются с помощью алгоритма SIMPLE толькд в жидкой области. Исследуются поле течения и распределение температур в объеме жидкости в процессе быстрого затвердевания алюминия и стали при различных величинах мощности лазера (10^8 и 10^9 Вт. м$^{-2}$) и времени взаимодействия. Наблюдается исчезновение течения вскоре после удаления лазерного луча. В случае с алюминием при высокой мощности объем жидкости сравнительно долго остается очень глубоким за счет образования крупного вторичного вихря в процессе плавления. Несмотря на различную форму границы раздела при наличии и отсутствии конвекции имеется незначительное различие во времени затвердевания для обоих металлов.